ECMWF Feature article

from Newsletter Number 120 – Summer 2009

METEOROLOGY

Improvements in the stratosphere and mesosphere of the IFS

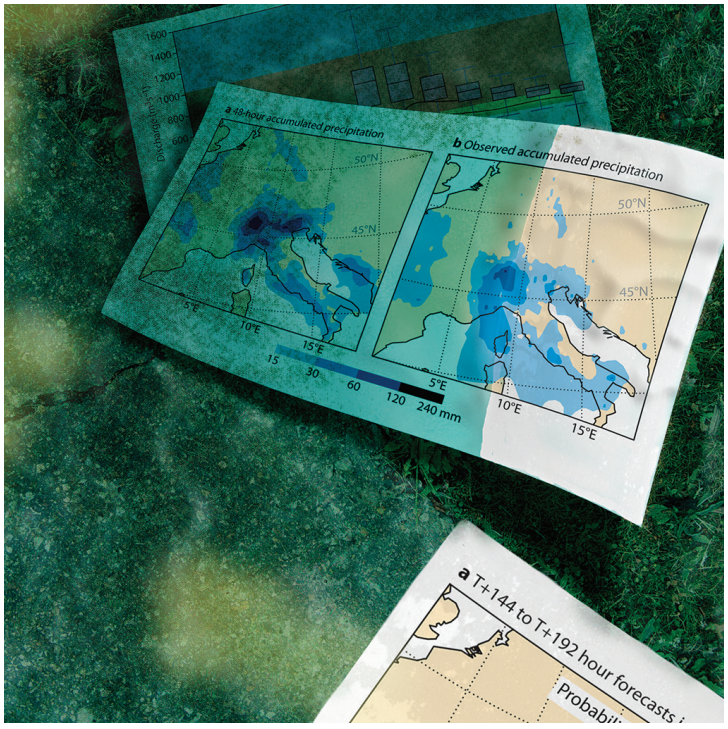

www.ecmwf.int/en/about/news-centre/media-resources

doi:10.21957/cs2g8q28uk

This article appeared in the Meteorology section of ECMWF Newsletter No. 120 – Summer 2009, pp. 22 -31.

Improvements in the stratosphere and mesosphere of the IFS

Peter Bechtold, Andrew Orr, Jean-Jacques Morcrette, Richard Engelen, Johannes Flemming, Marta Janiskova

In the middle atmosphere, which comprises the stratosphere and the mesosphere, the general circulation is driven by the processes of radiation and wave drag due to gravity waves and planetary waves. The term 'wave drag' is understood as the deceleration/acceleration of the flow due to breaking waves, as during the dissipation process waves 'drag' the flow towards their own horizontal phase speed.

The physics of the middle atmosphere is described in Box A. A key feature of the flow in the middle atmosphere is the formation of a strong westerly jet (referred to as the polar night jet) in the winter hemisphere with a weaker easterly jet in the summer hemisphere. The speed of these jets is limited by the drag exerted on the horizontal winds by dissipating quasi-stationary planetary waves and gravity waves that originate in the troposphere. The quasi-stationary vertically-propagating planetary waves occur mainly in the northern hemisphere due to their orographic origin. These waves are resolved by the model dynamics. The orographic gravity waves emanating from the model-resolved orography are explicitly represented whereas those linked to the subgrid orography are parametrized.

Non-orographic gravity waves are generated by mechanisms such as deep convection, frontal instabilities, shear zones and thermal contrasts. The term non-orographic implies that these waves are non-stationary (i.e. have non-zero phase speeds). Ground-based and aircraft observations of the waves are available, and recently global data on the wave properties and the associated momentum fluxes have been obtained from infrared radiation measurements onboard satellite by *Ern et al.* (2004) during the CRISTA campaign. It is found that the vertical wavelengths of the waves vary from a few hundred metres to tens of kilometres, and the horizontal wavelengths from tens to thousands of kilometres Therefore, these waves are generally unresolved or under-resolved by the model and/or their generating mechanism cannot be represented by the model. Consequently, their impact on the middle atmosphere circulation must be parametrized. In this article the implementation of such a parametrization scheme in the ECMWF Integrated Forecast System (IFS) is described.

Parametrization of non-orographic gravity wave drag

Until model cycle Cy35r2 (operational since 10 March 2009) the IFS did not make use of a parametrization scheme for non-orographic gravity wave drag (NOROGWD), but instead above 1 hPa so called Rayleigh friction has been applied – this is a simple deceleration of the flow proportional to the zonal mean wind speed. A parametrization scheme for non-orographic gravity waves has been introduced in Cy35r3 (becoming operational in summer 2009) following the scheme developed by *Scinoccia* (2003) that is itself based on the approach of *Warner & McIntyre* (1996).

The physical principles behind the parametrization scheme are simple and similar to most operational parametrizations. At a certain level in the troposphere a spectrum of waves is emitted in the four main directions (north/south, east/west), having a broad range of vertical wavelengths and frequencies. The launch spectrum is assumed to be independent of time and localisation. For practical reasons computations are performed using horizontal phase speeds instead of frequencies, and the wave package is represented by the total wave momentum flux or Eliassen-Palm flux rather than the total wave energy. The wave package then undergoes conservative vertical propagation until partial dissipation takes place due to two processes:

- ***Critical level filtering.*** This occurs when the phase speed of the waves approaches the ambient wind speed. The process requires realistic model winds. It is particularly effective when the wind speed changes sign (e.g. when waves emitted in the tropospheric westerlies meet stratospheric easterly winds).
- ***Non-linear dissipation.*** As the amplitude of the waves increases with height due to the decrease in density, the growth of the gravity wave spectrum at large wavenumbers (short waves) is bounded so as not to exceed some 'saturated' spectrum.

 doi:10.21957/cs2g8q28uk

The scheme requires a few important parameters, namely the shape and amplitude of the wave spectrum at the launch level, the saturation level for the larger vertical wavenumbers, and the launch-level height. The latter is of particular importance as it determines the Doppler shift of the departure wave spectrum by the ambient wind. For the parameter setting we essentially followed *Ern et al.* (2006) who evaluated a version of the Warner and McIntyre scheme against satellite measurements of wave momentum flux during the CRISTA campaign.

The departure level of the waves is set to 450 hPa, and the amplitude of the wave momentum flux is set to a globally constant value of 3.75×10^{-3} Pa. The functional shapes for the unsaturated and saturated part of the spectrum are given in Figure 1, where the characteristic vertical wavenumber m^* separating the two distinctive parts of the spectrum corresponds to a vertical wavelength of 2 km. The unsaturated (long wave) part of the spectrum is naturally less well known as it is difficult to measure. Each time the spectrum exceeds the dashed line in Figure 1 the non-linear dissipation is supposed to occur and the corresponding amount of momentum flux is removed and deposited into the environment. There is one free parameter in the scheme that allows the shifting of the saturation line in Figure 1, and therefore determines the height where non-linear dissipation occurs - this has important consequences for the stratospheric oscillations.

Finally, numerical aspects had to be considered as NOROGWD schemes tend to be computationally expensive with computing times in the range of 15–20% of the total model run time (*Scinoccia,* 2003). For this purpose we reduced the number of spectral intervals to 20 from 50 originally proposed, reduced the calling frequency to 1 or 2 hours (depending on model resolution), and optimised the coding structure. This meant that, without any significant loss of numerical accuracy, the NOROGWD scheme contributes to less than 3% to the total forecast run time.

Physics of the middle atmosphere

A

The climatological temperature and wind profiles of the atmosphere for July at latitude 40°S are shown in the figure along with the distribution of the 91 model vertical layers of the IFS.

The temperature decrease with height in the troposphere is due to adiabatic decompression, and the westerly jet in the middle latitudes of the upper-troposphere is generated by the horizontal temperature gradient between the tropical and polar latitudes.

The stratosphere is characterised by an increase in temperature as infrared radiative cooling is offset by heating through the absorption of solar radiation by greenhouse gases, mainly ozone.

Above the stratopause, in the mesosphere, the ozone heating decreases with height, and so does the temperature. The radiative heating has a strong latitudinal variation, with a maximum in the summer polar region and a minimum in the winter polar region. The resulting horizontal temperature gradient between the summer hemisphere and the winter hemisphere creates a meridional circulation, with air rising at the summer pole and sinking at the winter pole. The Coriolis torque acting on the meridional circulation leads in the winter hemisphere to the formation of a strong westerly jet, the so called polar night jet, that peaks at the stratopause at 1 hPa, and can locally attain monthly mean wind speeds of over 100 m s^{-1} in the southern hemisphere. A weaker easterly jet forms in the summer hemisphere. The only force that can balance the Coriolis torque, and therefore limit the horizontal winds, is the drag exerted by dissipating quasi-stationary planetary waves and gravity waves that originate in the troposphere.

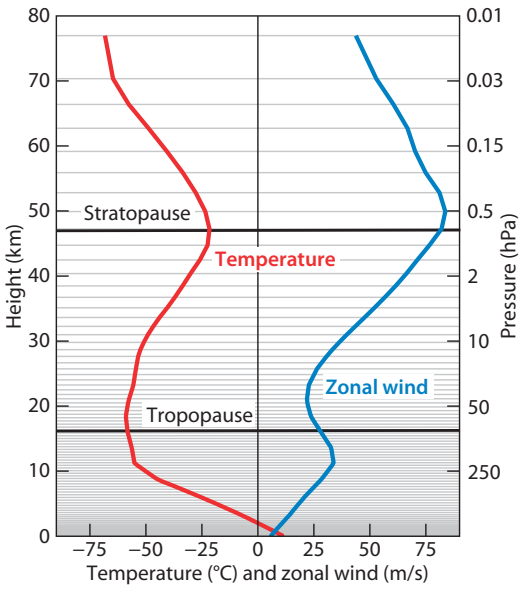

Climatological atmospheric temperature and zonal wind profiles for July at latitude 40°S. The thin horizontal lines mark the 91 vertical layers of the IFS. ***Troposphere:*** extends from the surface to roughly 100 hPa (0–15 km) and is represented by 51 model layers. ***Stratosphere:*** extends from 100 hPa to 1 hPa (15–48 km) and is represented in the IFS by 31 model layers. ***Mesosphere:*** extends from 1 hPa to 1 Pa (48–80 km) and contains 9 model layers in the current IFS. The top of the mesosphere, the mesopause, corresponds also to the top of the IFS.

doi:10.21957/cs2g8q28uk

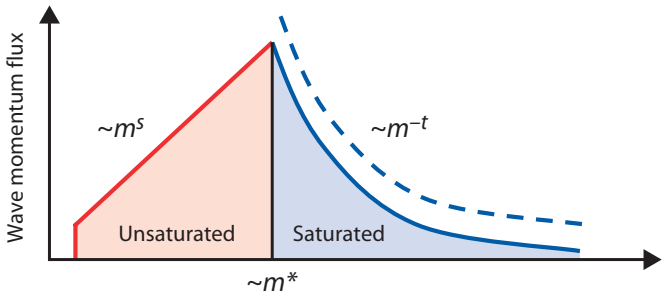

Figure 1 Spectrum of wave momentum flux at the departure level as a function of vertical wavenumber m. The unsaturated and saturated parts are denoted by the red and blue line, respectively, with $s = 1$ and $t = 3$. The characteristic wavenumber m^* typically corresponds to a vertical wave length of 2 km. The dashed line denotes the saturation spectral density. All values are scaled by a fixed amplitude.

Trace gas concentrations

The radiative heating/cooling rates of the middle atmosphere strongly depend on the trace gas concentrations. A list of the relevant trace gases, with the exception of ozone, is given in Table 1. Before Cy35r2 the concentrations for these species have been simply specified as constants following the IPCC/SACC Climate Change 1995 Report (*Houghton et al.,* 1995). The ozone, a quantity that strongly varies with height, has been given by monthly evolving two-dimensional climatological fields as a function of pressure and latitude following *Fortuin & Langematz* (1994).

The most important greenhouse gases are carbone dioxide (CO_2), ozone (O_3) and methane (CH_4). Concentrations for these three gases have been replaced in Cy35r3 by new monthly evolving two-dimensional climatologies computed from the GEMS reanalysis that is available so far for the period 2003–2007 (GEMS is an EU-funded project concerned with global and regional Earth system monitoring using satellite and in situ data). For the missing species, such as the nitrogen oxides and the chlorofluorocarbons, we now use two-dimensional climatologies computed from the two-dimensional chemical transport model MOBYDIC by D. Cariolle at Météo-France.

The GEMS derived CO_2 and O_3 climatologies were taken from the year 2006 (when microwave limb sounder data was available O_3) and the CH_4 analysis was taken from the year 2005. These datasets represent the best fit to available observations. Furthermore, the CO_2 and CH_4 climatological fields are trend corrected to account for the man-made increase in greenhouse gas concentrations since 1850.

In order to compare the concentrations in Cy35r3 to the constant values used before Cy35r2, typical global annual mean concentrations have been computed as given in Table 1. One notices the significantly higher CO_2 and CH_4 values in Cy35r3 compared to Cy35r2. Furthermore, as an example, zonal cross-sections of the CO_2 and O_3 mixing ratios for July and January (representative for the year 2006) are illustrated in Figure 2. The CO_2 concentrations vary between 564×10^{-6} and 591×10^{-6} kg kg^{-1} (371–389 ppmV) with maximum values occurring in the northern hemisphere troposphere. But there is a strong seasonal cycle, and high mixing ratios are also present throughout the tropical troposphere and lower stratosphere due to surface emissions by biomass burning and subsequent vertical convective mixing. In contrast, the O_3 mixing ratios peak in the stratosphere and this leads to strong radiative heating due to the absorption of solar ultraviolet radiation. Peak concentrations of 18×10^{-6} kg kg^{-1} (10.86 ppmV) are attained in the tropical upper-stratosphere between 5 and 15 hPa.

Trace gas	Cy35r2	Cy35r3
CO_2	536 (353)	584 (384)*
CH_4	0.953 (1.72)	0.957 (1.73)*
N_2O	0.471 (0.31)	0.478 (0.31)
NO_2	0.794×10^{-4} (0.500×10^{-4})	1.896×10^{-4} (1.194×10^{-4})
CFC_{11}	1.328×10^{-3} (0.280×10^{-3})	1.169×10^{-3} (0.247×10^{-3})
CFC_{12}	2.020×10^{-3} (0.484×10^{-3})	2.151×10^{-3} (0.515×10^{-3})

Table 1 Trace gas concentrations in units of kg kg$^{-1}\times10^{6}$, and in parentheses in units of parts per million by volume (ppmV), as used until Cy35r2, and typical annual and atmospheric mean values for Cy35r3 computed from the new climatology that is given as monthly evolving zonal mean fields. Asterisks in Cy35r3 denote values that have been computed from the GEMS reanalysis.

doi:10.21957/cs2g8q28uk

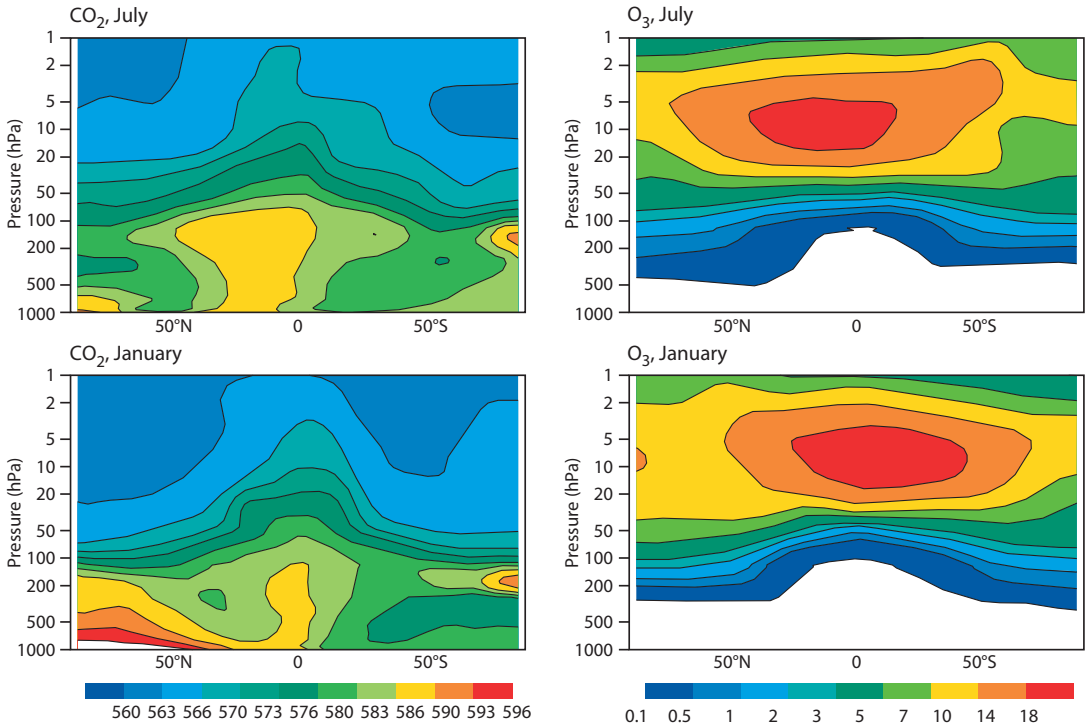

Figure 2 Zonal mean climatological concentrations (kg kg^{-1}×10^{6}) for CO_2 and O_3 from the GEMS reanalysis during July and January.

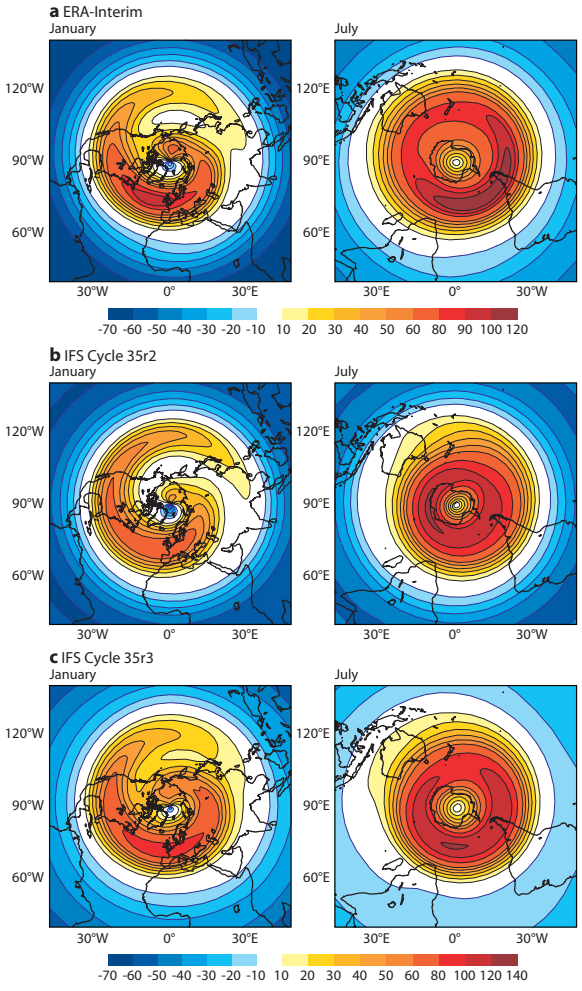

Figure 3 Zonal mean wind speed (m s^{-1}) at 1 hPa for the northern hemisphere polar vortex during January (left column) and the southern hemisphere polar vortex during July (right column) averaged over the period 1993–1998 from (a) the ERA-Interim, (b) Cy35r2, and (c) Cy35r3. The symmetry of the vortex is disrupted in the northern hemisphere by quasi-stationary Rossby waves.

doi:10.21957/cs2g8q28uk

Climatology

The SPARC (Stratospheric Processes And their Role in Climate) climatology (www.atmosp.physics.utoronto.ca/ SPARC/) can be taken as an independent reference dataset for the middle atmosphere, and therefore can be used for model evaluation. Alternatively, one could derive a climatology from the operational ECMWF analysis and reanalysis such as ERA-Interim. However, before Cy35r2, including ERA-Interim, the analysis is not constrained by observations in the mesosphere. Only since Cy35r2, with the introduction of the radiative transfer model RTTOV9, is the operational analysis in the mesosphere weakly constrained by data, mainly from IASI satellite infrared channels onboard MetOp. Furthermore, the ERA-Interim dataset is limited to 0.1 hPa. Therefore, we primarily evaluate the model's middle atmosphere climatology against SPARC, although stratospheric wind data from the ERA-Interim reanalysis will also be considered.

The stratospheric wintertime polar vortex is illustrated in Figure 3 at the 1 hPa level for the northern hemisphere during January (left column) and the southern hemisphere during July (right column). The reanalysis data is compared to the model climatologies of Cy35r2 and Cy35r3 which are obtained for the period 1993–1998 from an ensemble of six one-year forecasts at resolution T159 (125 km) with analysed sea surface temperatures.

ERA-Interim (Figure 3a) shows a quasi-symmetric southern hemispheric polar vortex with maximum monthly mean wind speeds of 120 $m\,s^{-1}$. The northern hemispheric polar vortex, by contrast, is weaker and strongly disrupted over the Pacific due to vertically propagating large-scale quasi-stationary Rossby waves.

The-ERA Interim data is reasonably reproduced with model Cy35r2 (Figure 3b). However, the southern hemispheric vortex is too strong and too narrow, and underestimates the local jet maximum between Africa and South America. For the northern hemispheric wintertime vortex, on the contrary, the jet maxima over the North Atlantic are underestimated by up to 20 $m\,s^{-1}$, and the wind speeds over the Pacific are overestimated by 10 $m\,s^{-1}$.

Cy35r3 (Figure 3c) generally improves the representation of both the northern and southern polar vortex, and is also able to reproduce the local jet maxima. In particular the representation of the jet between Africa and South America during austral winter, as well as the jet over the North Atlantic and Europe during boreal winter, is improved.

Figure 4 shows cross-sections of monthly mean temperature and zonal wind for July from SPARC along with the corresponding model results with Cy35r2 and Cy35r3.

The comparison between SPARC and Cy35r2 for July (Figures 4a and 4b) reveals a 10–20 K warm bias around the stratopause. Also apparent are a 25 K warm bias with Cy35r2 around the northern polar (summer) mesopause and a 10 K cold bias at the southern polar (winter) mid-stratosphere, indicative of an atmosphere with an overturning circulation that is too weak. Furthermore, the south polar wintertime jet is too strong in Cy35r2 and lacks the observed vertical inclination towards the tropics. Also, the mesospheric jet in the northern summer hemisphere is too weak and its core is near the stratopause instead of being located near the mesopause. This bias is directly related to the use of Rayleigh friction formulated in terms of a damping coefficient which increases with height, and which therefore strongly damps any upper-level winds.

In contrast, comparison of SPARC and Cy35r3 (Figures 4a and 4c) shows that Cy35r3 corrects most of the deficiencies of Cy35r2. In particular the temperature structure in the upper stratosphere and mesosphere is improved, and the stratospheric polar winter jet and the mesospheric polar summer jet now present reasonable inclinations with the jet cores at the right height. The reduced temperature errors around the stratopause are due to the improved greenhouse gas climatology, whereas the reduced temperature and wind errors in the mesosphere are a consequence of the strong NOROGWD tendencies in the mesosphere (Figure 5). These decelerate the southern (winter) hemisphere westerly jet with a rate of up to 80 $m\,s^{-1}\,day^{-1}$ and also decelerate the northern (summer) hemisphere easterly jet. Overall the results for Cy35r3 represent a significant improvement over previous cycles, but the temperature at the stratopause is still overestimated by 5 K compared to SPARC and the tilt of the polar night westerly jet towards the tropics is underestimated.

A similar picture as for July is obtained for January (Figure 6) but with the wind directions in each hemisphere reversed. Again, Cy35r2 produces a too warm stratopause, a too warm summer polar summer mesopause, and a misplaced core of the summer polar mesospheric jet. The (northern) hemisphere wintertime polar jet is generally much weaker than the southern polar wintertime jet which explains the smaller differences between SPARC and Cy35r2 compared to Figure 4. Again Cy35r3 improves most of the deficiencies of Cy35r2 in the mesosphere and the upper stratosphere. However, the temperature at the stratopause is still too high compared to SPARC and the strength of the polar wintertime jet is overestimated.

 doi:10.21957/cs2g8q28uk

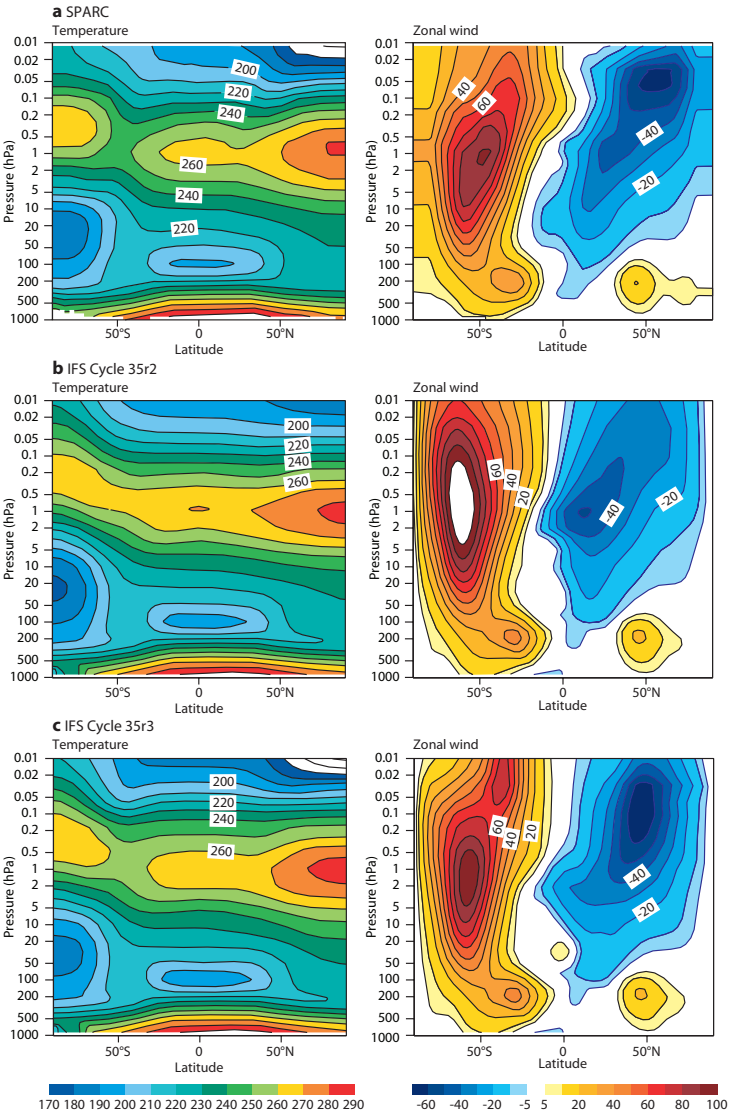

Figure 4 Zonal mean cross-section (latitude versus pressure) of temperature (K, left column) and zonal wind ($m\,s^{-1}$, right column) for July from (a) the SPARC climatology, and from an ensemble of one-year T159 integrations for the period 1993–1998 with (b) Cy35r2 and (c) Cy35r3.

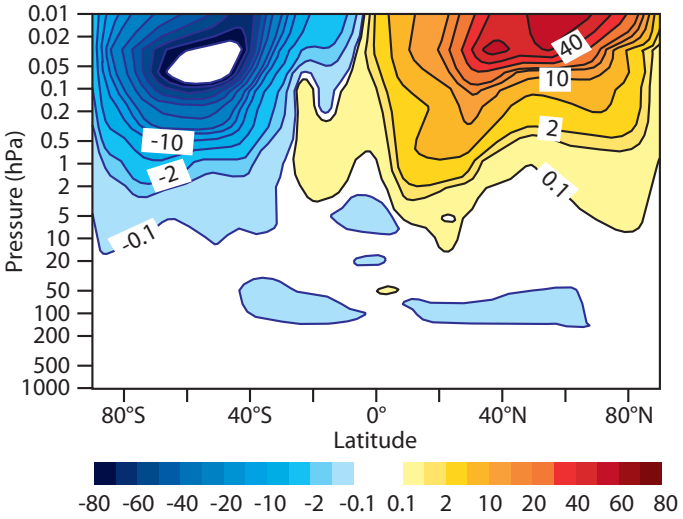

Figure 5 Zonal mean cross-section of the acceleration/deceleration ($m\,s^{-1}\,day^{-1}$) of the zonal wind during July due to the NOROGWD.

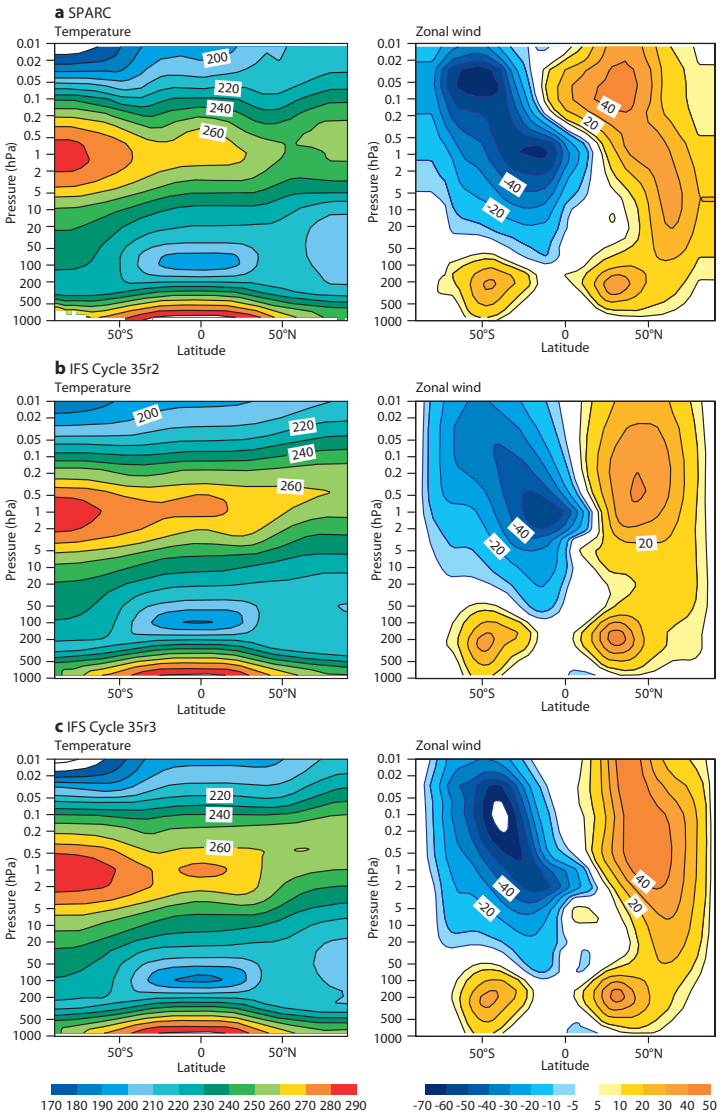

Figure 6 Zonal mean cross-section (latitude versus pressure) of temperature (K, left column) and zonal wind ($m\,s^{-1}$, right column) for January from (a) the SPARC climatology, and from an ensemble of one-year T159 integrations for the period 1993–1998 with (b) Cy35r2 and (c) Cy35r3.

Quasi-biennial oscillation

Concerning the variability of the tropical stratosphere, a prominent feature is the quasi-biennial oscillation (QBO) of the zonal wind that is also clearly evident from ERA-Interim (Figure 7a) with amplitudes on the order of +20 to –40 $m\,s^{-1}$. The quasi semi-annual oscillation of the stratosphere and the lower mesosphere is also present in the reanalysis data. The downward propagation of these oscillations results from breaking gravity waves that deposit momentum near critical levels, thereby changing the zonal winds; this in turn leads to a downward propagation of the critical level.

The ability of the IFS to produce the quasi semi-annual oscillations has been verified with the aid of multi-year integrations. Results for Cy35r2 (Figure 7b), and all previous cycles, show that these cycles have not been able to produce realistic stratospheric oscillations, but instead only produce easterly tropical stratospheric winds that do not propagate downward beyond the 30 hPa level. In contrast, with Cy35r3 (Figure 7c) clear downward propagating oscillations are present with a realistic amplitude that on average extend downward to 60–80 hPa but sometimes even extend to the lower stratosphere and upper troposphere. However, the period of the QBO-like oscillations in Cy35r3 is about 1.3 years, and therefore significantly shorter than that observed.

As shown in Figure 7d, it is possible to simulate the desired period using Cy35r3 by shifting the saturation spectrum in Figure 1 to the right (i.e. to higher wave numbers). These results are consistent with sensitivity studies reported in the literature which showed that shifting the wave saturation, and therefore momentum deposition, to higher levels in the mesosphere leads to a more realistic representation of the period of the QBO. Unfortunately, the latter option could not be retained for the operational cycle Cy35r3 as it leads to problems in the temperature and wind fields at the model top through excessive momentum deposition.

doi:10.21957/cs2g8q28uk

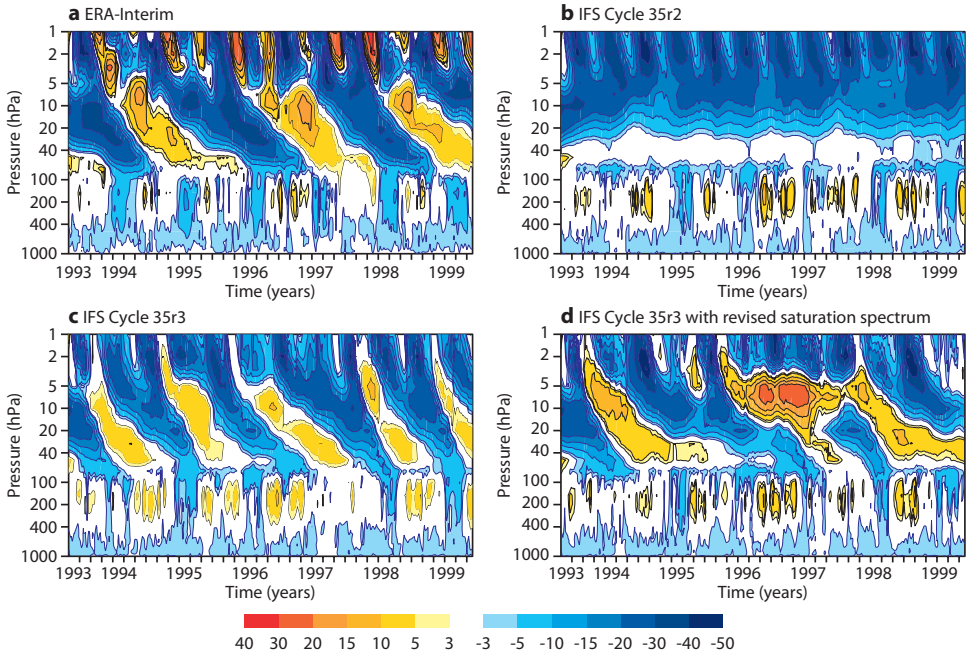

Figure 7 Hovmöller plots (pressure versus time) of the six-year evolution of the zonal wind speed ($m\,s^{-1}$) averaged over the tropical band 10°S–10°N from (a) ERA-Interim , and from six-year integrations with (b) Cy35r2, (c) Cy35r3, and (d) Cy35r3 but with the saturation spectrum for the non-linear gravity wave drag dissipation shifted to higher wavenumbers. ERA-Interim shows a biannual oscillation in the stratosphere, and a semi-annual oscillation in the upper part of the stratosphere and the mesosphere.

High-resolution analysis suite

The introduction of a parametrization for the non-orographic gravity wave drag, and a more realistic greenhouse gas climatology in Cy35r3 leads to substantial improvements in the mean circulation and variability of the middle atmosphere. These improvements are also evident from pre-operational analysis cycling performed with Cy35r3.

The analysis part of Cy35r3 contains another important contribution to the middle atmosphere. Until Cy35r2 the use of the linearized long-wave radiation scheme has been restricted to the troposphere. This was necessary in order to avoid spurious noise and deterioration in the tangent linear approximation. However, in Cy35r2 a linearized version of the full long-wave radiation code has been implemented. As this new linear scheme also allows for radiative tendency perturbations in the middle atmosphere, we decided that Cy35r3 should make use of the temperature perturbations due to long-wave radiation throughout the atmosphere. This improves the tangent linear approximation, and makes potentially better use of middle atmosphere observations.

In Figure 8 the mean errors for temperature and zonal wind for August 2008 of the 72-hour deterministic high-resolution T799 (25 km) forecasts with Cy35r1, Cy35r2 and Cy35r3 have been computed with respect to the own analysis of each cycle.

In Cy35r1 (Figure 8a), which was the operational cycle during that period, large model errors existed in the winter mesosphere with mean temperature and wind errors exceeding 20 K and 25 $m\,s^{-1}$, respectively. Also the stratopause is apparent as a region with a warm bias of a few K.

In Cy35r2 (Figure 8b) the errors in the upper mesosphere (the uppermost four model layers) have been significantly reduced compared to Cy35r1 due to a better usage of satellite observations the mesosphere with the introduction of the RTTOV9 radiative transfer model.

Finally, with Cy35r3 (Figure 8c) the errors in the mesosphere and upper stratosphere are further reduced. The smaller warm bias around the stratopause, in particular, is due to the new greenhouse gas climatology, whereas the reduction in the mesospheric wind errors has been obtained due to the NOROGWD. There are, however, still problems concerning the upper-stratospheric winds in the tropics, a too strong polar night jet with a too small tilt toward the tropics, and the cold bias in the lower stratosphere has increased by about 0.5 K compared to previous cycles. Overall the medium-range forecast errors with respect to the own analysis are similar to the errors seen in long integrations with respect to SPARC (Figure 4c).

There is some positive impact of Cy35r3 on classical tropospheric scores in the middle latitudes in the medium range. One could expect that, on monthly and seasonal time scales, the middle atmosphere changes, in particular the changes to the polar stratospheric vortex and the more realistic stratospheric oscillations in the tropics, would have an even larger influence on the tropospheric predictions. We do not yet have enough evidence from numerical experimentation to test this hypothesis as currently the improvements in the middle atmosphere analysis and deterministic forecast are not reflected in the operational ensemble monthly and seasonal forecasts which make use of a 62-level configuration with a model top at 5 hPa.

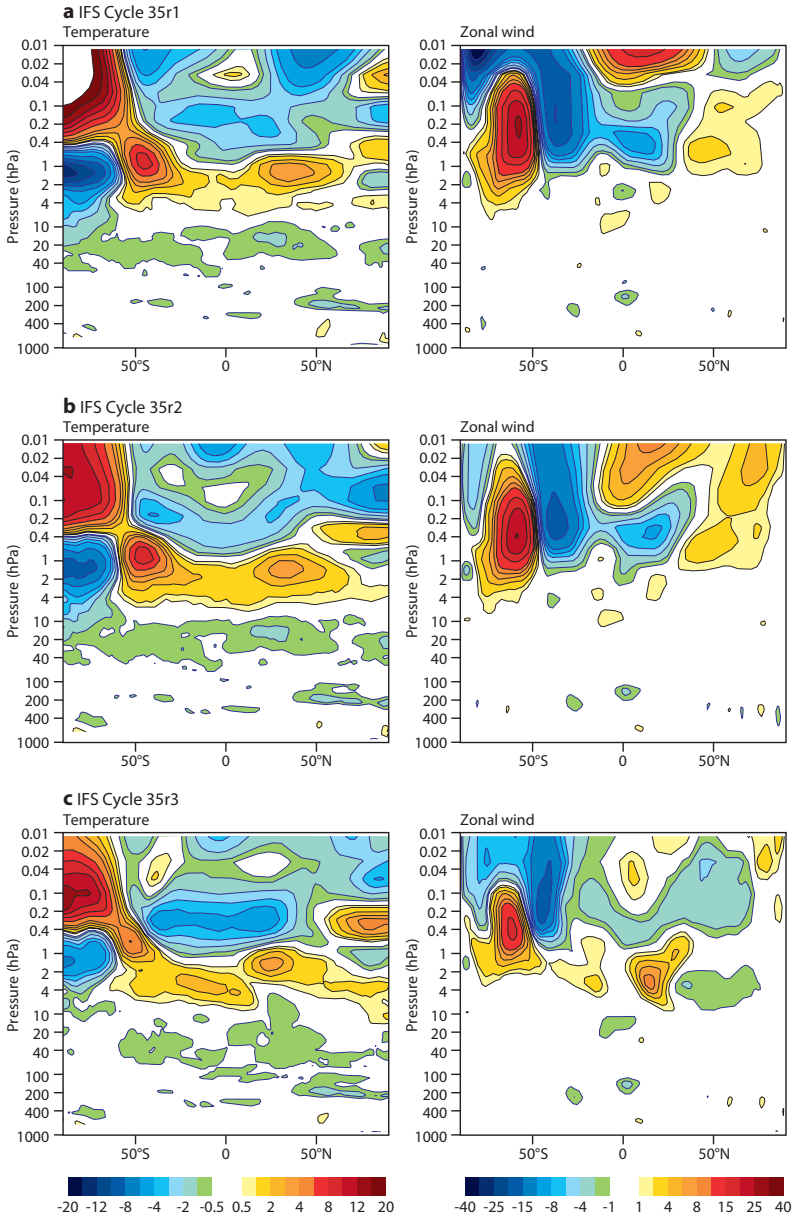

Figure 8 Cross-sections of errors in mean temperature (K, left column) and zonal wind ($m\,s^{-1}$, right column) during August 2008 of the 72-hour deterministic high-resolution forecasts with (a) Cy35r1, (b) Cy35r2 and (c) Cy35r3. Each cycle is verified against its own analysis.

doi:10.21957/cs2g8q28uk

Further improvements

There is still room for further improving the circulation in the middle atmosphere. One should keep in mind that the NOROGWD scheme uses a globally uniform launch spectrum, and only allows for vertical propagation of gravity waves. It therefore provides a rather simplified representation of the actual generation and oblique propagation of gravity waves. Furthermore, the planned model upgrades in horizontal resolution (late 2009) and vertical resolution (2010) might help to better represent the resolved gravity waves.

Lifting the model top, which in the current high-resolution forecast system is located at the mesopause, could help avoid problems caused by wave reflection from the upper boundary that are noticeable in the tropics. However, an extension of the model into the lower thermosphere would be difficult to realise as it requires modifications to the radiation scheme due to the non-equilibrium radiative processes which become relevant at these altitudes.

Finally, we are also looking forward to the vertical-resolution upgrade of the ensemble prediction system in 2010 which will allow, together with the current physics upgrade, a more realistic representation of the stratosphere/troposphere interactions on monthly to seasonal timescales.

Further reading

Ern, M., P. Preusse, M.J. Alexander & **C.D. Warner,** 2004: Absolute values of gravity wave momentum flux derived from satellite data. *J. Geophys. Res.,* **109,** D20103, doi:10.1029/2004JD004752

Ern, M., P. Preusse & **C.D. Warner,** 2006: Some experimental constraints for spectral parameters used in the Warner and McIntyre gravity wave parameterization scheme. *Atmos. Chem. Phys.,* **6,** 4361–4381.

Fortuin, J.P.F. & **U. Langematz,** 1994: An update on the global ozone climatology and on concurrent ozone and temperature trends. Proceedings SPIE. *Atmos. Sensing and Modelling,* **2311**, 207–216.

Houghton, J.T., L.G. Meira Filho, B.A. Callander, N. Harris, A. Kattenberg & **K. Maskell Eds.,** 1995: IPCC/SACC Climate Change 1995 Report, *Cambridge University Press.*

Scinoccia, J.F., 2003: An accurate spectral nonorographic gravity wave drag parameterization for general circulation models. *J. Atmos. Sci.,* **60,** 667–682.

Warner, C.D. & **M.E. McIntyre,** 1996: On the propagation and dissipation of gravity wave spectra through a realistic middle atmosphere. *J. Atmos. Sci.,* **53,** 3213–3235.

doi:10.21957/cs2g8q28uk